Available online at www.sciencedirect.com
ScienceDirect
International Journal of Heat and Fluid Flow 28 (2007) 988–1002
International Journal of HEAT AND FLUID FLOW
www.elsevier.com/locate/ijhff

Infrared thermography investigation of local heat transfer in a plate fin and two-tube rows assembly

D. Bougeard *

Ecole des Mines de Douai, Département Energétique Industrielle, 941 rue Charles Bourseul, B.P. 10838, 59508 Douai Cedex, France

Received 3 June 2006; received in revised form 30 January 2007; accepted 31 January 2007
Available online 26 March 2007

Abstract

An experimental study is performed using an infrared thermography system. The experimental method uses the temperature transient variation of a thin plate (tested fin) in order to obtain detailed quantitative heat transfer coefficients. The method developed is similar to the lumped capacitance method usually used to measure heat transfer coefficient on heat exchanger fin models. But the method presented here exploits the capabilities of infrared thermography to measure surface temperatures in a transient technique in order to take into account errors effects due to tangential conduction and radiation of the tested fin. The method is validated using a two-dimensional channel experiment and its advantages are highlighted using a plate fin and two-tube rows assembly experiment. Moreover, convection coefficient variations with fin pitch and frontal air velocity of an automotive plate fin and two-tube rows assembly are also examined.

Keywords: Fin and tube heat exchanger; Convection heat transfer; Infrared thermography

1. Introduction

Plate finned-tube heat exchangers are intensively used in many industrial processes. The performances of this kind of heat exchanger are directly linked to the air-side thermal resistance. On the air side, the heat transfer surface is usually expanded using continuous fins. Automotive heat exchangers often consist of two rows of round tubes geometry with continuous or louvered fins. The fluid flow structure between the fins depends strongly on the geometrical parameters, inline or staggered tube arrangements, tube spacing, tube shape, tube diameter and fin spacing. Moreover, alternative enhancement techniques consisting in punching out of the fins some vortex generators that strongly modify the fluid flow structure also exist (see Jacobi and Shah, 1995 for details). Hence in order to determine the best geometrical arrangement one needs to get precise heat transfer coefficient distribution on the fin surface.

Several research groups have designed experimental methods to examine local heat transfer rate in tube finned geometries. Kim and Song (2002) use a naphthalene sublimation technique to investigate local heat transfer in a plate fins/circular tube assembly. The authors show the great importance of the vortex structure developed in front of the tube, called horseshoe vortex (HSV), on the overall heat transfer coefficient. When the Reynolds number is large enough, they also found that a smaller subsidiary vortex appears attached to the main one. While the naphthalene sublimation technique uses a heat and mass transfer analogy to determine local heat transfer coefficients, other researchers develop experimental thermal methods. Tiggelbeck et al. (1992) use a thermal transient method that exploits time temperature variation of a thin plate suddenly heated by convection using warm air. The convection coefficient is deduced using a time integration of the energy equation using the three following assumptions: conduction and radiation heat fluxes are negligible, and

* Tel.: +33 3 27 71 23 74; fax: +33 3 27 71 29 15.
E-mail address: bougeard@ensm-douai.fr

0142-727X/$ - see front matter © 2007 Elsevier Inc. All rights reserved.
doi:10.1016/j.ijheatfluidflow.2007.01.008

Nomenclature

C_p	specific heat, kJ kg^{-1} K^{-1}
D	tube diameter, m
D_h	hydraulic diameter based on twice fin spacing, m
e_f	fin thickness, m
E	fin spacing, m
$h_{(x,y)}$	local heat transfer coefficient (Eq. (5)), W m^{-2} K^{-1}
$h_{\log(x,y)}$	local heat transfer coefficient based on lumped capacitance method (Eq. (3)), W m^{-2} K^{-1}
I_{cond}	energy per unit area exchanged by lateral conduction in the fin (Eq. (7)), J m^{-2}
I_{total}	total energy per unit area exchanged by the fin (Eq. (6)), J m^{-2}
I_{rad}	energy per unit area exchanged by radiation (Eq. (8)), J m^{-2}
I_{temp}	time integration of temperature difference (Eq. (9)), K s
L	longitudinal length of the fin, m
Pt	transverse tube pitch, m
Pl	longitudinal tube pitch, m
s	spacing between pixel, m
t	time, s
t_{init}	initial time of acquisition, s
t_{final}	final time of acquisition, s
T	temperature, K
Tm	time averaged temperature, K
T_{rad}	reference temperature for radiation heat transfer, K
T_{ref}	reference temperature for convection heat transfer, K
x	space coordinate along airflow, m
y	space coordinate transverse to the airflow, m

Greek symbols

ε	emissivity
ϕ	heat flux density, W m^{-2}
λ	thermal conductivity, W m^{-1} K^{-1}
Δt	time duration between two consecutive images, s
ρ	density, kg m^{-3}
σ	Stefan–Boltzmann constant, W m^{-2} K^{-4}

Subscripts

cond	conduction heat transfer
conv	convection heat transfer
f	refer to the fin
rad	radiation heat transfer
span-mean	refer to span averaged value

Abbreviations

CFD	computational fluid dynamics
HTC	heat transfer coefficient
HSV	horseshoe vortex
IR	infrared
LCM	lumped capacitance method

temperature is constant along the plate thickness. This last assumption is usually assumed to be correct if the Biot number is under a value of 0.1. The integrated energy equation then lead to a very simple equation with two measured local temperatures of the thin plate (see Eq. (3)).

Very recently, Kim et al. (2006) used the same method and validated it with quantitative measurement in plate fin and tube heat exchanger. In this last paper, the authors claim that the lumped capacitance method is reliable in comparison with usual transient method. Anyway, in all those papers, several points limit the accuracy of the convection coefficient determination. The assumption of negligible lateral conduction is always made. Even if those conduction fluxes are usually low, there can exist regions of the analysed surface where the convection coefficient variations induce high heat conduction fluxes within the tested plate. Furthermore, the tested plate used in liquid crystal experiments is a composite medium of a thin polycarbonate plate, and two more layers: a liquid crystal material and a black paint. This set-up of different materials can have an influence on the thermal behaviour of the tested plate.

Quantitative infrared thermography is a very powerful technique for temperature measurements. Several authors used infrared camera as a fruitfully way of determining heat transfer coefficient. In Astarita et al. (2000), the authors show the capability of infrared thermography to deal with convective heat transfer measurements in complex fluid flow configurations. Several methods of convective heat transfer coefficient determination are analysed in the paper. Usually, for subsonic experiments the method used is a steady-state condition method (known as *heated-thin-foil technique*).

Ay et al. (2002) used infrared thermography to measure local heat transfer coefficient on heat exchanger fins. These authors used also a steady-state technique that supplied a heat flux and measured precisely the heat transfer surface temperature. The main advantages of infrared camera are: a very high signal to noise ratio (modern camera have noise equivalent temperature difference less than 0.1 °C), the high scan speed (number of image per second), the valuable spatial resolution and the fact that the measurement is non-intrusive (except a black coating which is usually laid on the heat transfer surface).

Few authors used infrared thermography in transient technique using the lumped capacitance assumption. Tourreuil (2002) used an infrared set-up for determining heat transfer coefficient on heat exchanger geometry. The aim of his study is to investigate heat transfer distribution on fin and tube assembly in order to compare it with fluid flow

investigations in such geometry. Fluid flow investigations are performed using CFD simulations (Khallaki et al., 2005) and particle image velocimetry (PIV) experimentations (Nacer-Bey et al., 2002).

In this paper we present a transient method for heat transfer coefficient measurements using an infrared set-up. In this technique, the infrared camera measures the temperature variation (in space and time) of a thin polycarbonate plate. The originality of our technique is that unlike precedent authors, the method of convection coefficient determination uses the entire time variation of surface temperature during cooling process. Moreover, it allows the determination of quantitative convection coefficient taking into account conductive (lateral conduction) and radiative fluxes. Moreover, the technique is used to perform heat transfer measurement in a plate fin and two-tube assembly with frontal air velocity and fin pitches variations.

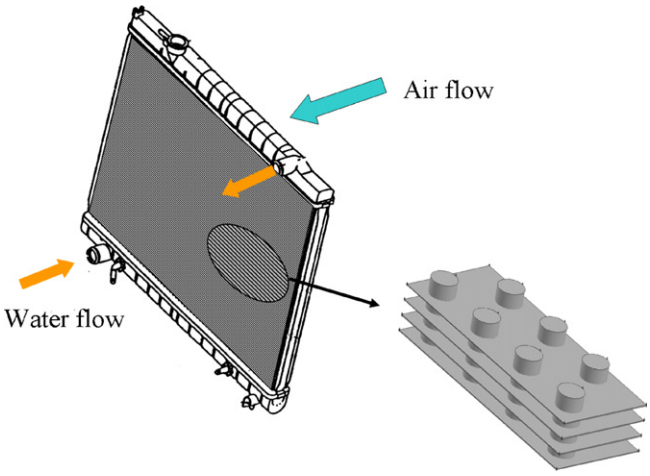

Fig. 1. Plate fin-and-tube radiator.

2. Experimental test bench

In the automotive industry, the engine-cooling radiator consists of arrays of finned tube. In this system wasted heat from the engine is transferred to the surrounding air that is forced through a closely spaced mesh of cooling fins that are heated by the circulating cooling liquid (see Fig. 1). The fins can be mechanically fixed to the tubes. While this work concerns only the analysis of air-side heat transfer, the performance of those devices is examined using a simplified plate fin-tube assembly.

2.1. Test model geometry

The airside elementary pattern of the heat exchanger is composed of two staggered rows of tube (streamwise direction) bounded with symmetry planes (see Fig. 2). The test model geometry is a plate fin-tube assembly composed of one fin and circular acrylate disks fixed on each side of it. In order to enhance spatial resolution of the experimental measurements, the test model is scaled up. In the experiments, the test model is inserted into a wind tunnel. The airflows is driven through the two ducts bounded by the fin and the wind tunnel walls (Fig. 2). In order to simulate the symmetry plane S1 and S2 of the airflow, several circular disks are placed spanwise (Figs. 3 and 4). The upstream airflow will be considered as uniform.

2.2. Experimental facility description

The experimental facility is schematically illustrated in Fig. 3. It is designed to investigate heat transfer performance of plate fin and two-tube rows assembly placed in the test section of a subsonic blow-down open circuit wind tunnel. The test section consists of a rectangular duct of 450 mm width and variable height in order to test different model's fin spacing. The test model is composed of a thin polycarbonate foil with cylindrical disk modelling the two

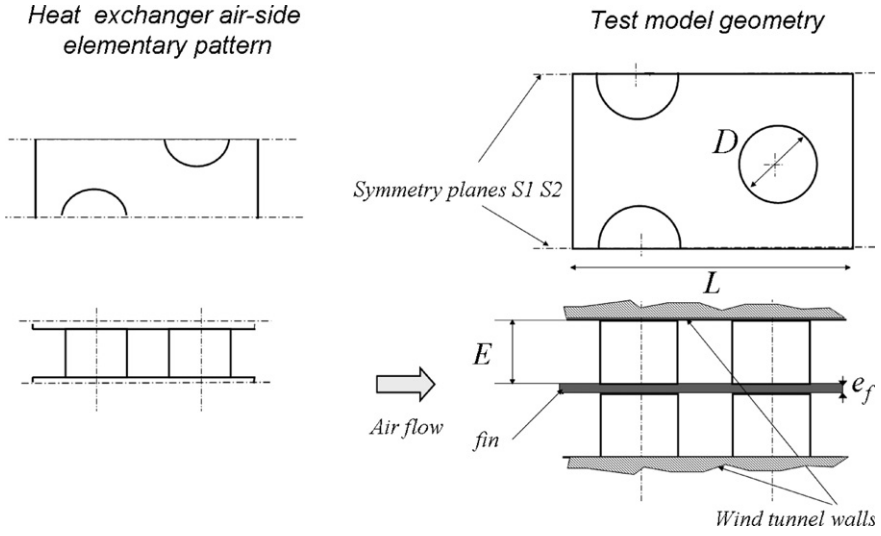

Fig. 2. Test model geometry.

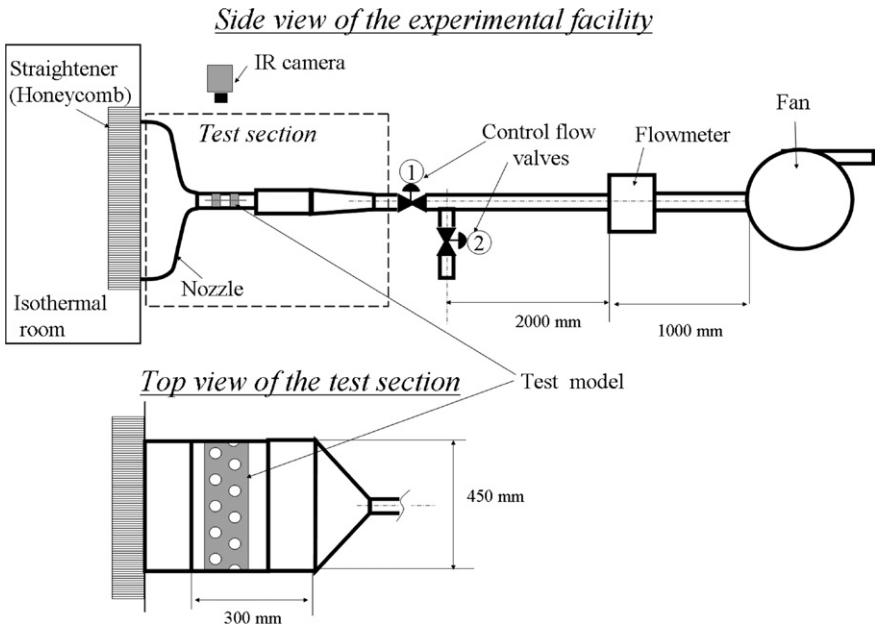

Fig. 3. Schematic diagram of the experimental apparatus.

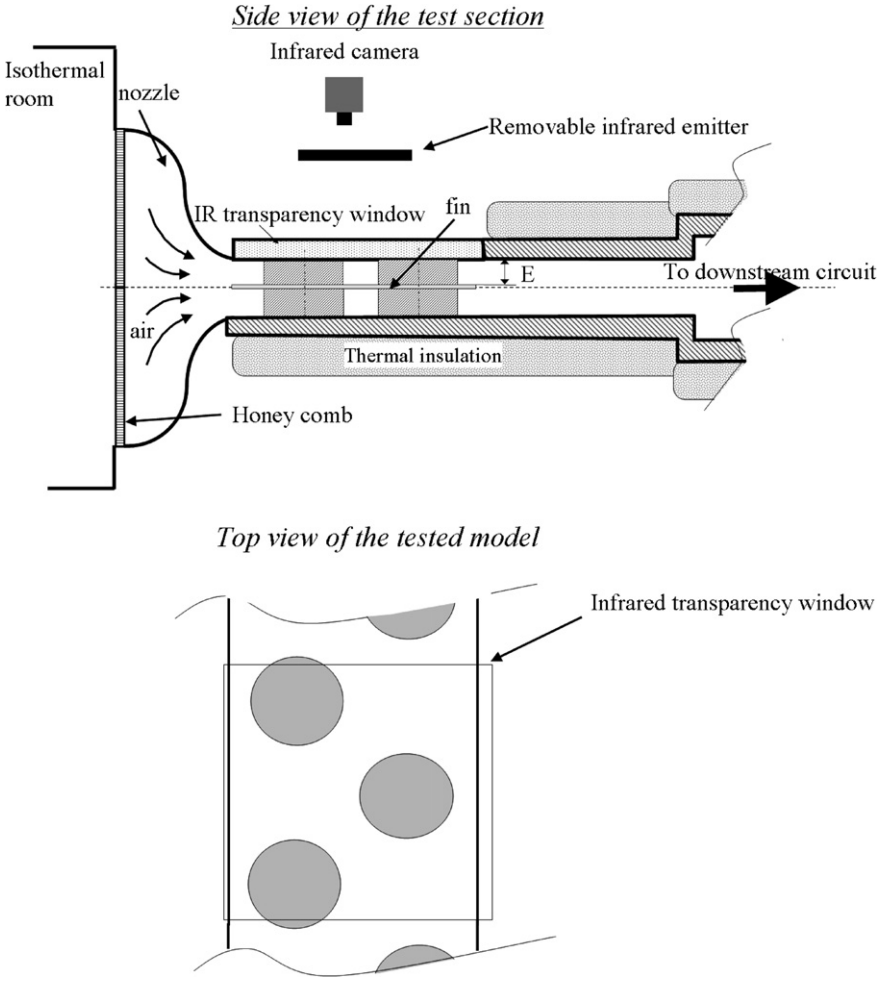

Fig. 4. Detailed view of the test section.

rows fin-an-tube assembly. A blower is used to produce the airflow in the wind tunnel. The air, flows from an isothermal room to the test section through a honeycomb and a nozzle. In the downstream circuit, a system of two flow control valves and a by-pass line allow the pumping of air either inside or outside the isothermal room. The air is finally ducted to a flowmeter, before being discharged into the atmosphere by a fan.

The inlet contraction which have a 20:1 area reduction, is designed using the correlation given by Morel (1977). The design gives a quasi-uniform velocity profile at the inlet of the test section. This uniformity was checked through laser Doppler velocity measurements (Tourreuil, 2002).

As previously said, the test model is a scaled-up model of the real prototype. The fin pitch value, E, of the scaled up model takes three different values 7–9–12 mm (Fig. 4). An infrared camera is placed above the duct in order to measure the temperature field of the fin surface trough an IR transparent window. The visualised area is shown in Fig. 4.

2.3. Temperature measurements by infrared thermography

The temperature field on the polycarbonate fin is measured using an infrared thermography set-up. A long wave infrared camera with a 10° lens is placed at the minimal focalisation distance above the model. A window made of a special material (ZnSe) transparent in the long wave range infrared radiation allows quantitative IR thermography. The window has a direct transmission factor of 98% between 8 and 12 μm IR wavelength. The infrared scanner is the AGEMA® Thermovision 900 system with an HgCdTe detector sensitive in the 8–12 μm wavelengths range and cooled by a Stirling engine. The scanning mechanism of the camera allows a scan speed (frame rate) of 15 non-interlaced frames per second (15 Hz). The analog signal acquired by the infrared camera is processed by a specific high accuracy signal-conditioning unit (ADDELIE®). The signal-conditioning unit working principle, is illustrated in Fig. 5. Firstly an offset voltage, which is approximately equal to the time-mean value output signal of the camera, is subtracted from the analog signal of the IR camera. The transformed signal is then amplified using an adjustable gain, so that the fluctuating output signal from the conditioning unit nearly cover the complete Analog to Digital Converter voltage range. Finally, the signal is digitized by the 12-bits converter (i.e., 4095 values). It is important to note that this signal conditioning allows an accurate adaptation of the time temperature variation amplitude of the thermal scene, during the test, to the whole 12 bits resolution of the system.

2.4. Temperature calibration

To calibrate the temperature measurement we use an in-situ technique. A special high conductivity plate coated with the same high emissivity coating (about 0.94) as the fin, is placed at the same location (Fig. 6) in the test section. This calibration plate can this way be considered very closed to an ideal blackbody with very low reflection. The calibration copper plate has inner water circulation (not completely presented in Fig. 6) with a temperature regulation using a high accuracy regulated temperature water bath (0.01 °C of temperature stability), and a thermal probe. The calibration process links the uniform

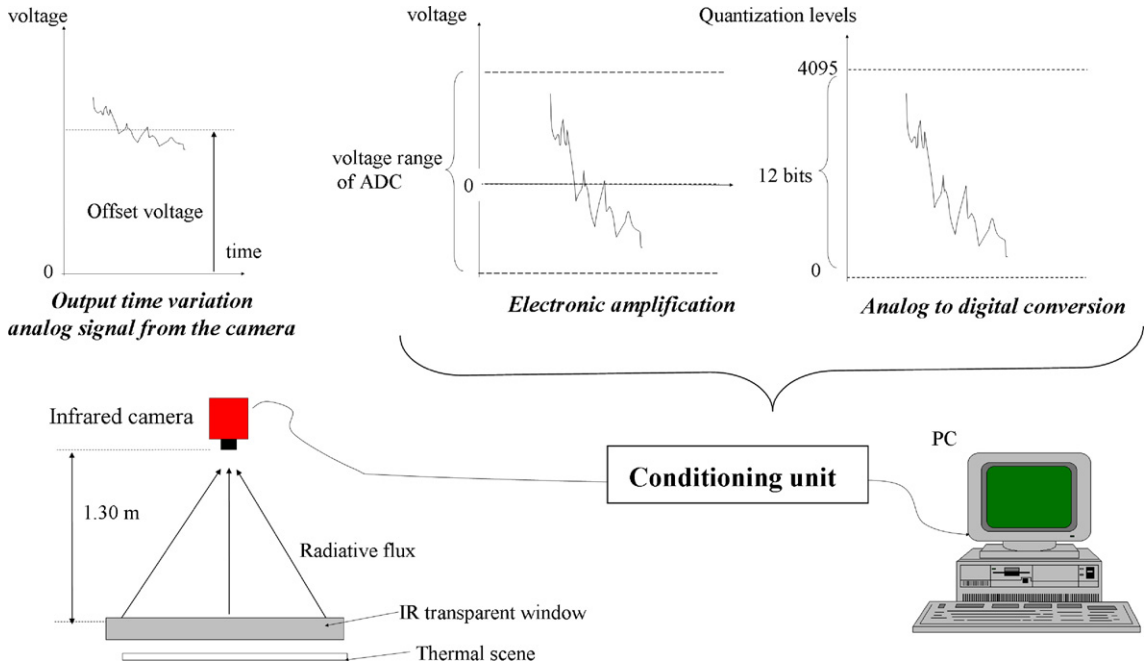

Fig. 5. Infrared signal conditioning.

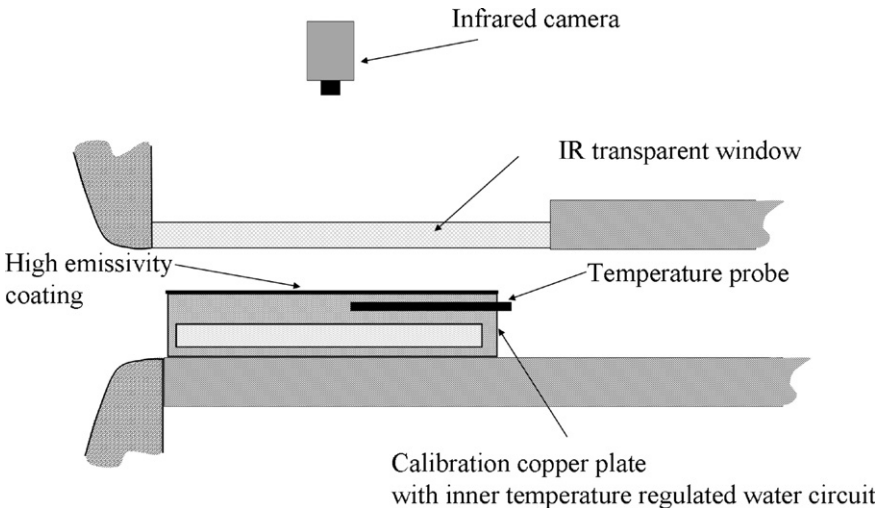

Fig. 6. Calibration process.

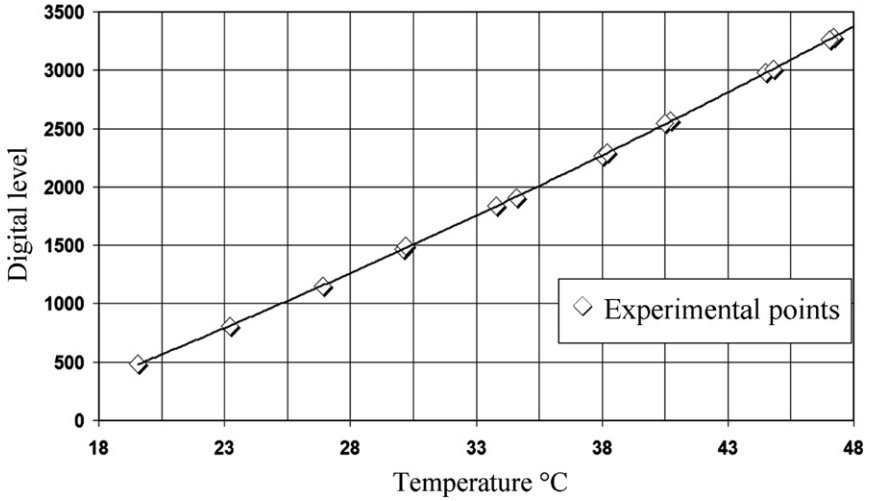

Fig. 7. Calibration curve.

temperature of the calibration plate and the signal given by the thermography system. The resulting calibration curve is given in Fig. 7. The temperature range is chosen to fit the temperature variation occurring during the test. Each test configuration requires a specific calibration curve. This technique allows accurate measurements of the fin temperature with an overall uncertainty equal to ±0.15 °C.

2.5. Spatial resolution

An important characteristic and major limitation of infrared systems is the spatial resolution. Considerable effort has been made to enhance spatial resolution of our thermography system. Infrared scanners using a single detector give a smooth image of the thermal scene. If high spatial frequencies signals exist in the thermal scene, the IR scanner may certainly lower those signals amplitude. In order to limit this phenomenon we placed the camera at its minimal focalisation distance. More over a specific digital image restoration technique was developed to enhance spatial resolution. The restoration technique uses a two-dimensional Wiener filter. Details on this technique can be found in Bougeard et al. (1994). Finally, our system is capable of measuring sharp spatial variation of temperature on the thermal scene up to three pixels width with little smoothing. In Fig. 8, we present the dimension of the scaled-up plate fin/tube assembly with the spatial digitizations.

3. Experimental method

3.1. Heat transfer coefficient calculation

The experimental method is inspired by the work of Kim et al. (2006) and Tourreuil (2002). In those authors' previous works, the experimental process consists in suddenly

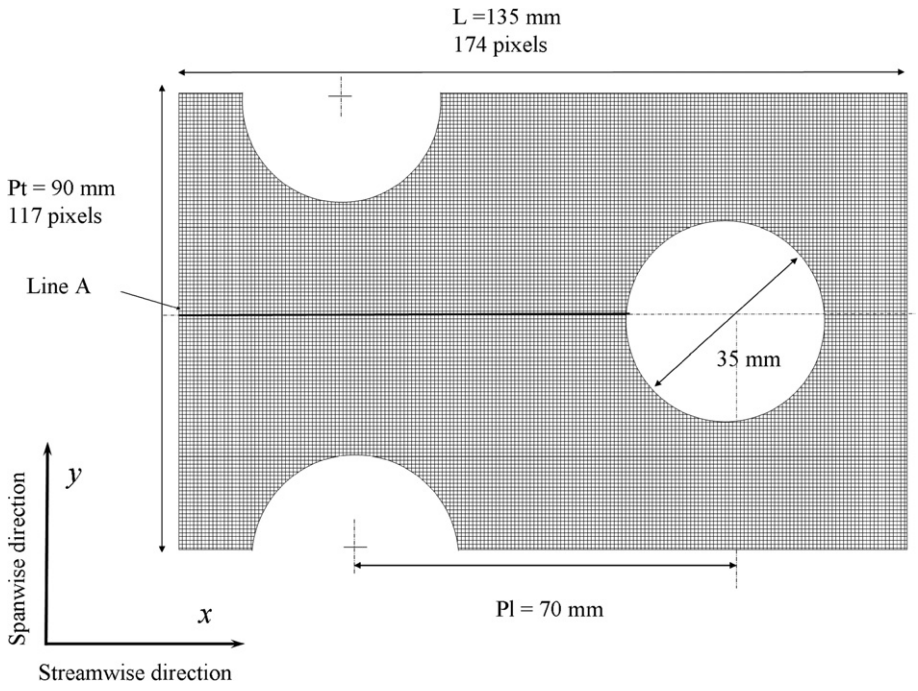

Fig. 8. Spatial digitization.

warming up (or cooling down) an experimental model by convection. The local convection coefficient is then deduced from the local time variation of temperature of the model. The mathematical calculation of the heat transfer coefficient from the temperature time variation is based on the "lumped capacitance method" (LCM) reported by Incropera and Dewitt (2002). The time evolution of the experimental model temperature is regarded as the response of a thin body to a sudden change in surrounding convection condition. For example, if we consider a thin plate at an initial temperature, suddenly cooled by forced convection, the heat fluxes balance of the thin plate gives (Fig. 9)

$$\rho_f \cdot C_{p_f} \cdot e_f \cdot \frac{dT_{(x,y,z,t)}}{dt} = \phi_{conv} + \phi_{cond} + \phi_{rad} \quad (1)$$

If we make the assumption that the temperature gradient across the plate thickness (z-direction) is negligible ("lumped capacitance method") it gives

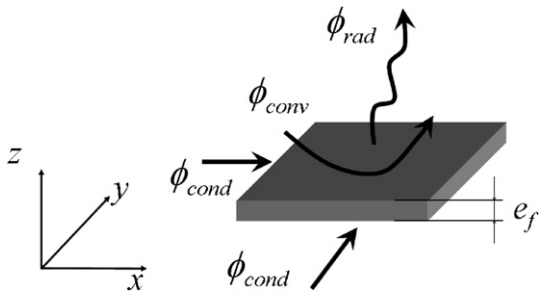

Fig. 9. Heat flux balance on a thin body.

$$\rho_f \cdot C_{p_f} \cdot e_f \cdot \frac{dT_{(x,y,t)}}{dt} = h_{(x,y)} \cdot (T_{(x,y,t)} - T_{ref}) + \lambda_f \cdot e_f \cdot \left(\frac{\partial^2 T}{\partial x^2} + \frac{\partial^2 T}{\partial y^2}\right) + \varepsilon \cdot \sigma \cdot (T^4_{(x,y,t)} - T^4_{rad}) \quad (2)$$

where T_{ref} and T_{rad} are respectively reference temperatures used to calculate convection and radiant fluxes between the plate and its surrounding.

Generally, authors (Tiggelbeck et al., 1992; Kim et al., 2006 or Tourreuil, 2002) add the following assumptions: negligible heat conduction within the wall and negligible radiation heat transfer. Given this, the heat transfer coefficient can finally be derived from Eq. (2) after time integration between initial time t_{init} (plate at uniform temperature) and final time t_{final} with a cooling duration equal to $(t_{final} - t_{init})$:

$$h_{(x,y)} = \frac{\rho_f \cdot C_{p_f} \cdot e_f}{2(t_{final} - t_{init})} \cdot \ln\left(\frac{T_{ref} - T_{(x,y,t_{init})}}{T_{ref} - T_{(x,y,t_{final})}}\right) = h_{\log(x,y)} \quad (3)$$

One can see from this last equation that the measurement of the heat transfer coefficient requires only the acquisition of two-temperature fields at t_{init} and t_{final}. The main advantage of the method is its simplicity in the calculation of $h_{\log(x,y)}$. Anyway, the two simplification assumptions may provide strong errors depending on the convection coefficient values. High variations of heat transfer coefficients (along x- and y-axes) can imply significant heat conduction fluxes inside the plate. Furthermore, low values of heat transfer coefficient can increase the proportion of radiation heat transfer. For all those reasons the method presented here does not use those simplification hypotheses and

makes a direct integration of Eq. (2) between the two instants t_{init} and t_{final}:

$$\rho_{\text{f}} \cdot C_{p_{\text{f}}} \cdot e_{\text{f}} \cdot \int_{t_{\text{init}}}^{t_{\text{final}}} \frac{\mathrm{d}T_{(x,y,t)}}{\mathrm{d}t}\mathrm{d}t = h_{(x,y)} \cdot \int_{t_{\text{int}}}^{t_{\text{final}}} \left(T_{(x,y,t)} - T_{\text{ref}}\right)\mathrm{d}t + \lambda_{\text{f}} \cdot e_{\text{f}} \cdot \int_{t_{\text{init}}}^{t_{\text{final}}} \left(\frac{\partial^2 T}{\partial x^2} + \frac{\partial^2 T}{\partial y^2}\right)\mathrm{d}t + \varepsilon \cdot \sigma \cdot \int_{t_{\text{init}}}^{t_{\text{final}}} \left(T^4_{(x,y,t)} - T^4_{\text{rad}}\right)\mathrm{d}t \quad (4)$$

The experimental set-up gives the values of plate temperature on m discrete instants with a temporal image frequency acquisition of 15 Hz, meaning a time duration Δt (equal to 0.067 s) between two consecutive pictures. The m images stored by the infrared set-up during the cooling period, allow the calculation of the local convection coefficient. The four time-integrals are numerically calculated. We note I_{total} the integral term corresponding of the total energy per unit area lost by the fin (left side of Eq. (4)), I_{cond} the conductive term of Eq. (4), I_{rad} the radiative term of Eq. (4), and I_{temp} the term corresponding of the time integration of the difference of fin temperature and T_{ref}. The local convection coefficient can be then deduced from the simple ratio:

$$h_{(x,y)} = \frac{I_{\text{total}} - I_{\text{cond}} - I_{\text{rad}}}{I_{\text{temp}}} \quad (5)$$

where

$$I_{\text{total}} = \rho_{\text{f}} \cdot C_{p_{\text{f}}} \cdot e_{\text{f}} \cdot \sum_{i=1}^{m} (T_i - T_{i+1}) \quad (6)$$

$$I_{\text{cond}} = \lambda_{\text{f}} \cdot e_{\text{f}} \cdot \Delta t \cdot \sum_{i=1}^{m} \left(\frac{\nabla^2 T}{4 \cdot s^2}\right) \quad (7)$$

with $\nabla^2 T$ the discrete Laplacian

$$\nabla^2 T = (T_{k-1,j} + T_{k+1,j} + T_{k,j-1} + T_{k,j+1}) - 4 \times T_{k,j}$$

$$I_{\text{rad}} = \varepsilon \cdot \sigma \cdot \Delta t \cdot \sum_{i=1}^{m} (T_i^4 - T_{\text{rad}}^4) \quad (8)$$

$$I_{\text{temp}} = \Delta t \cdot \sum_{i=1}^{m} (T_i - T_{\text{ref}}) = m \cdot \Delta t \cdot (Tm - T_{\text{ref}}) \quad (9)$$

The discrete integration terms I_{total}, I_{cond}, I_{rad}, I_{temp}, are function of the space coordinates x and y. The integration limits t_{init} and t_{final} can also be taken as function of space coordinate. This last solution can be used to have, for example, the same energy loss per unit area I_{total} for each point (x, y). Anyway, in this paper, all the following developments are made with same values of t_{init} and t_{final} for each point.

This method is a powerful way to determine the convection coefficient without too many simplification hypotheses. The only remaining hypothesis is that the convection coefficient is constant during the cooling period ($t_{\text{final}} - t_{\text{init}}$). The determination of the convection coefficient implies the measurement of two-reference temperatures T_{ref} and T_{rad}. In our tests, the convection reference temperature (T_{ref}) is set as the entrance temperature (temperature at the inlet of the wind tunnel). This temperature is measured during the cooling period using two thermocouples (Fig. 10(b)). The second reference temperature, T_{rad}, is used to calculate the heat losses by radiation of the fin during the cooling period. This temperature is measured using a thermocouple placed near the infrared window (Fig. 10). It is important to note that little difference exists between these two temperatures, which are close to ambient temperature.

The way of determining the convection coefficient previously described will be called hereunder 'integral method' ($h_{(x,y)}$ Eq. (5)). This method will be compared to the standard lumped capacitance method that determine the convection coefficient using only two temperature fields called $h_{\log(x,y)}$ (Eq. (3)).

3.2. Experimental process

The experimental process is divided in two periods. During the first period the blower is on and the first control

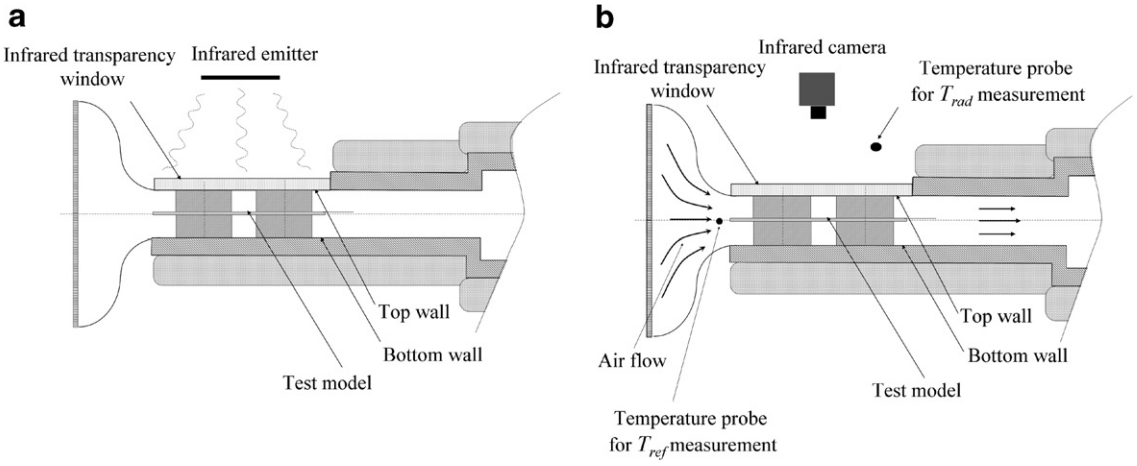

Fig. 10. (a) First period heating and (b) second period recording.

valve (1) is closed while the second control valve (2) is opened implying no airflow through the test section. A specific infrared emitting heater, heats up the fin through the infrared transparency window (Fig. 10(a)). In the second period, the infrared emitter is manually removed, and the first control valve is opened while the second control valve is closed steadying airflow in the test section. During the cooling period, the infrared set-up is used to record the temperature drop between initial instant t_{init} and final instant t_{final}. The infrared film acquired is treated afterward with our specific computer code written using Matlab™; the calibration function (see Section 2.4) is used to convert the IR signal into temperature; and the four integrals are calculated using Eqs. (6)–(9). Finally, the local convection coefficient $h_{(x,y)}$ is determined using Eq. (5).

3.3. Thermal boundary condition

During the heating process, only the fin is heated. The top and bottom walls (Fig. 10) are almost kept at ambient temperature, which is closed to the air reference temperature (less than 2 °C difference). During the cooling process, very little heat is transferred from the walls to the duct airflow so top and bottom walls are considered as adiabatic during the cooling period. To confirm this hypothesis, the temperature of the infrared window (which is the top wall) is measured using a thermocouple.

It is important to note that this thermal boundary condition is quite different from that of a real heat exchanger. In a real heat exchanger the inner channel is made of consecutive metallic fins with the same temperature field. Anyway, this difference has to be taken into account in order to compare our results with others experimental or CFD results.

4. Experimental validation of the HTC determination method

In a first step, in order to validate the complete experimental method we proceed to a validation test. The configuration chosen is an aerodynamically and thermally developing two-dimensional channel flow. Experimentally, the geometry analysed is the same as the plate fin-tube assembly except that the circular disks are removed and a special system fixed the fin on the sides of the wind tunnel. Hence, the fin (test model) remains located in the middle of the wind tunnel (Fig. 11).

The calculation of the reference convection coefficient is made using the well-known Stephan's empirical formula (Taine and Petit, 2003 or Bejan and Sciubba, 1992). This formula gives the mean Nusselt number (between 0 and x) for a developing duct flow with constant walls temperature. Because the thermal condition of the top wall of our set-up is adiabatic, the correlation cannot be strictly used to validate the method. To overcome this difficulty we have chosen specials conditions for the validation test that make negligible the influence of the thermal condition of the upper wall. In other words the test is performed with a sufficient frontal velocity and channel height (E) that keep the thermal boundary layer height, smaller than the mid height of the channel (all along the fin length (L) and during all the cooling period). A CFD simulation has been carried out to confirm the validity of this choice of parameters. (More details about the CFD study can be found in Tourreuil (2002).) Finally, the parameters values are a channel height of 7 mm and a Reynolds number equal to 1300. The comparison is presented in Fig. 12. The convection coefficient is span-averaged ($h_{span\text{-}mean}$) and compared with the convection coefficient determined using the previously published correlation. Span averaging is performed as a

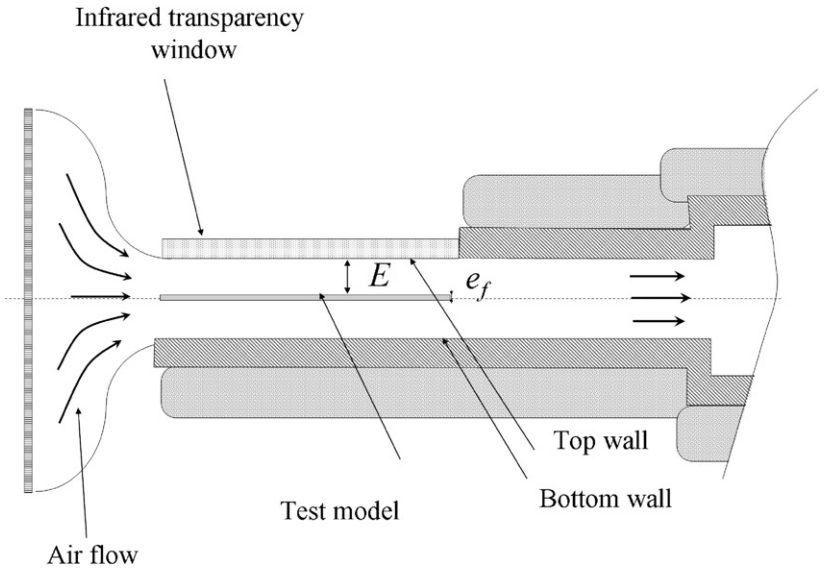

Fig. 11. Plate flow experiment configuration.

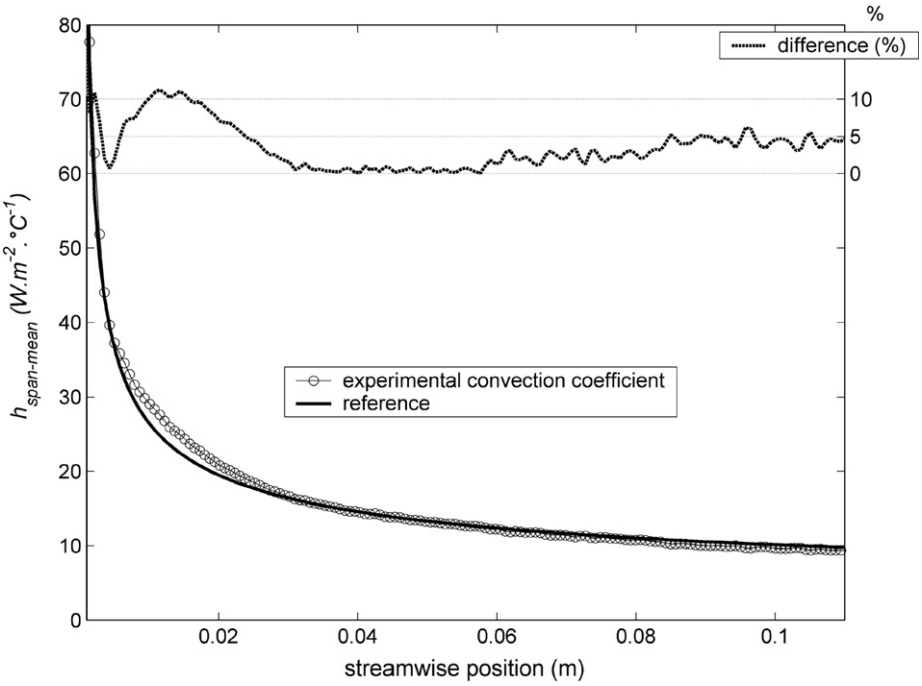

Fig. 12. Span-averaged convection coefficient for plate flow experiment.

simple arithmetic mean of the experimental points (pixels). The mean difference between the two curves is about 5% showing a very good agreement.

5. Plate fin and two-tube rows assembly experiments

5.1. Base case

In this chapter we present the analysis of the convective heat transfer for a base case. It consists of the two rows fin and tube assembly with a channel height of 7 mm and a frontal velocity equal to 1.5 m/s. According to the experimental process described in Section 3.2, the fin is previously warmed up to 42 °C and then cooled down by airflow with a fixed entrance temperature of 22 °C. The camera record temperature variations during a 6.5 s duration that represents one hundred thermal images. The four integral (I_{total}, I_{cond}, I_{rad}, I_{temp}) are calculated and the convection coefficient ($h_{(x,y)}$) deduced. In the next Fig. 13(a)–(e) we present the four integral results and the resulting convection coefficient spatial distribution.

The I_{total} image (Fig. 13(a)) represents the density of energy lost during the experiment (in J/m^2). High values are found at the leading edge due to the thin boundary layer beginning to be developed. High values are also found in front and around of the second tube row. These high values are the consequence of the horseshoe vortex (HSV) structure presence (as reported by many authors Khallaki et al., 2005; Nacer-Bey et al., 2002; Kim and Song, 2003). The I_{cond} image (Fig. 13(b)) reveals that high heat transfer by conduction exist around the tubes. As previously said this conduction heat transfer is due to high spatial variations of heat transfer coefficient due to the vortex structures (HSV). On the remaining part of the fin surface the conduction energy is roughly null, isolated sharp variations are due to the presence of noise in infrared images. The I_{rad} (Fig. 13(c)) image shows that radiation heat transfer is pretty low, representing only a few percents of the total energy exchange (an average value of 6% is often found). Anyway, downstream the tubes where the total energy exchange is very low (very low convection), the part of energy exchange by radiation is predominant.

The convection coefficient distribution (Fig. 13(e)), shows other interesting phenomena. First of all, the first row of tubes presents a very small HSV effect. Little increase of heat transfer is found in front of the first tube row. This phenomenon is well explained in Khallaki et al. (2005) and Kim and Song (2003) showing that the distance between the leading edge of the fin and the tube row has a major influence on the vortex structure development. If the distance is too short the vortex structure is not significant. Moreover, the staggering disposition of tube rows decreases the wake size behind the first tube row. This phenomenon was also shown by Kim and Song (2003) who tested different value of tube spacings. On the second rows of tubes, the HSV is magnified and composed of two vortices. This phenomenon has been first reported by Kim and Song (2002) who spoke about 'small subsidiary vortex attached to the main one'. Nacer-Bey et al. (2002) have performed detailed PIV analysis of the HSV structure around a tube inserted between two plates. They also reported that these two vortices structures depend on fin spacing and frontal velocity values. It must be emphasized that

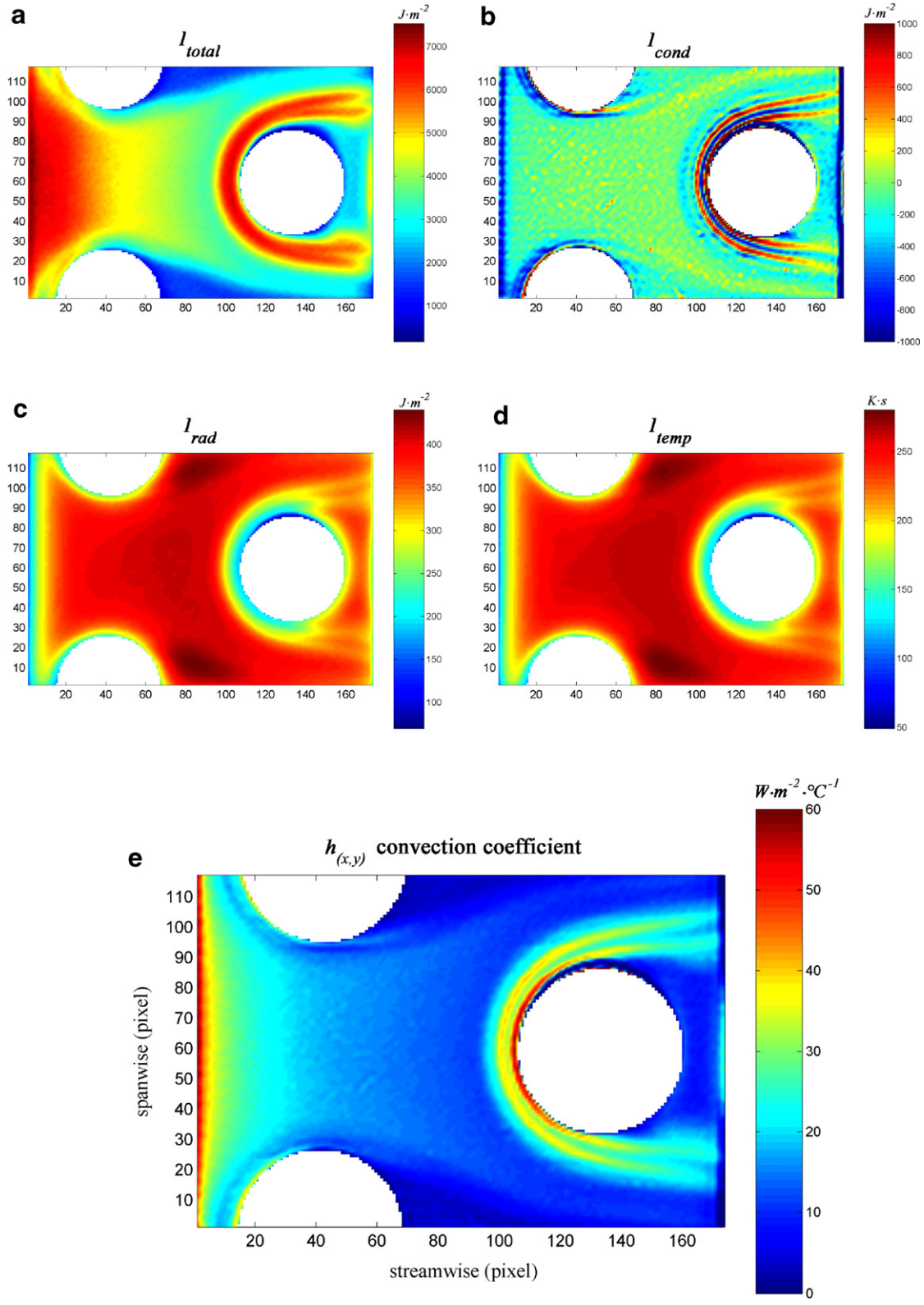

Fig. 13. Plate fin and two-tube rows assembly results (flow from left to right): (a) total energy exchanged, (b) energy exchanged by conduction, (c) energy exchanged by radiation, (d) temperature integration and (e) convection coefficient distribution.

the visualisation of this characteristic is possible because our method take into account the lateral conduction fluxes. To illustrate this remark we have calculated the convection coefficient with the ''standard'' lumped capacitance method (LCM) that we have called $h_{\log(x,y)}$ (calculated using Eq. (3)).

In Fig. 14, we present the convection coefficient distribution along the 'line A' (see Fig. 8) situated at a spanwise

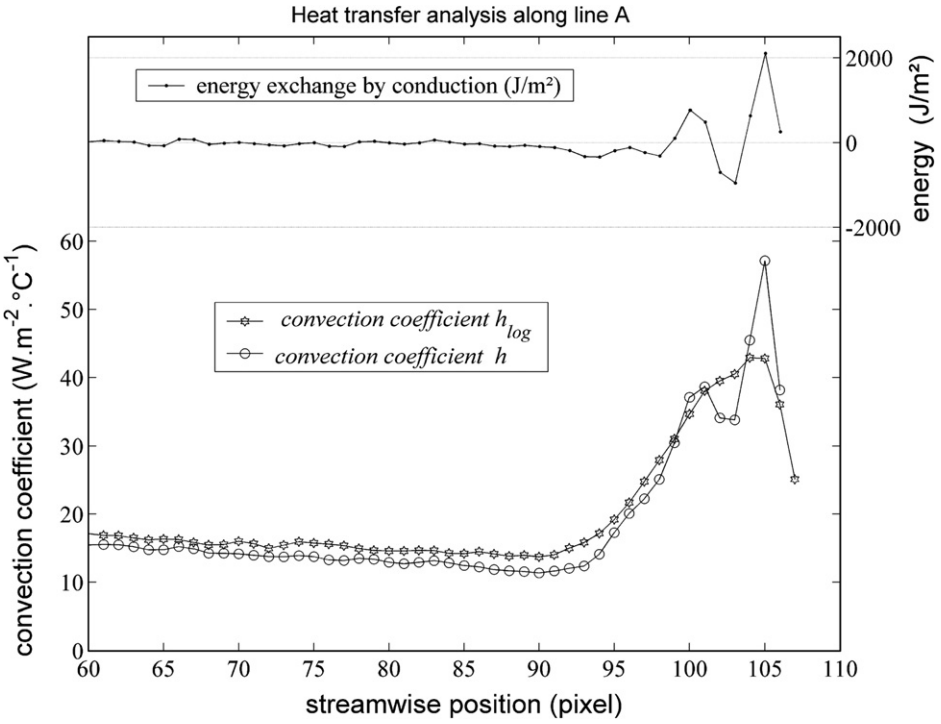

Fig. 14. Convection coefficient along line A (see Fig. 8) $y = 60$ (spanwise position in pixels) $h_{\log}$ (lumped capacitance method), h (integral method). The upper curve shows the local conduction heat exchange. Close to the second tube row (between pixels 95 and 107) high conduction heat exchange occur and modify the convection coefficient variation ($h_{(x,y)}$). The $h_{\log(x,y)}$ curve does not present those variations, only a smoother peak reveal the HSV influence.

position $y = 60$ (in pixel). The second row tube position is at pixel 107. Upstream this tube the two convection coefficients have quite similar values. The $h_{(x,y)}$ values are slightly lower than those of $h_{\log(x,y)}$ highlighting the influence of radiation exchange. Hence, the $h_{\log(x,y)}$ calculation overestimate the convection.

Close upstream the tube, we see in Fig. 14, that $h_{\log(x,y)}$ presents only one smooth peak. This is due to the fact that LCM interprets the loss of energy by lateral conduction as convection. So when high negative (the negative sign shows that energy is lost by the fin element, i.e., the fin is locally cooled down) energy is lost by lateral heat conduction (see the upper curve in Fig. 14), the LCM gives high (but wrong) values of $h_{\log(x,y)}$, overestimating convection phenomena. On the contrary when high positive conduction energy appears (energy is gained by the element, i.e., the fin is locally warmed up by conductive fluxes) the LCM underestimates the convection coefficient. This last point is well pointed out by the high convection coefficient found just upstream the tube with our method (Fig. 14). These remarks are key points showing the necessity of taking into account lateral conduction in the lumped capacitance method when accurate local description is needed. Indeed the assumption of negligible conduction heat fluxes is not always valid (even when Biot number is low) and this could explain why the double peak of heat transfer in front of a tube in plate fin-tube assembly is not always seen in precedent authors studies (Kim et al., 2006 or Tourreuil, 2002). As a conclusion, it is clear that the calculation of $h_{(x,y)}$ with our method give much more details than standard LCM determination ($h_{\log(x,y)}$) when high spatial variations of convection coefficient occur.

5.2. Variation of frontal velocity

Investigations of the influence of frontal air velocity on heat transfer have been performed for the base case geometry. Three different frontal velocities are set: 0.5 m/s, 1 m/s, 1.5 m/s. Fig. 15 shows the span-averaged heat transfer coefficient for the three velocities. The span average is calculated using numeric integration. Pt refers to spanwise dimension, for the fin-tube model the value of Pt depends on x-dimension because of the presence of tubes. Only the values of $h_{(x,y)}$ on the fin (not on the tubes) are taken in the averaging process:

$$h_{\text{span-mean}} = \frac{1}{Pt(x)} \int_{-Pt(x)/2}^{Pt(x)/2} h(x,y)\,\mathrm{d}y \tag{10}$$

When the frontal velocity increases (all other parameters being constant) the heat transfer is increasing. This fact is of course due to the natural increase of heat transfer with fluid flow velocity increase in the channel flow (Reynolds analogy). But another factor also influences heat transfer variation: the size and strength of the HSV (mainly for the second tube row). At each tube location (reported in Fig. 15) one can easily see that heat transfer enhancement is observed due to HSV presence, and that enhancement

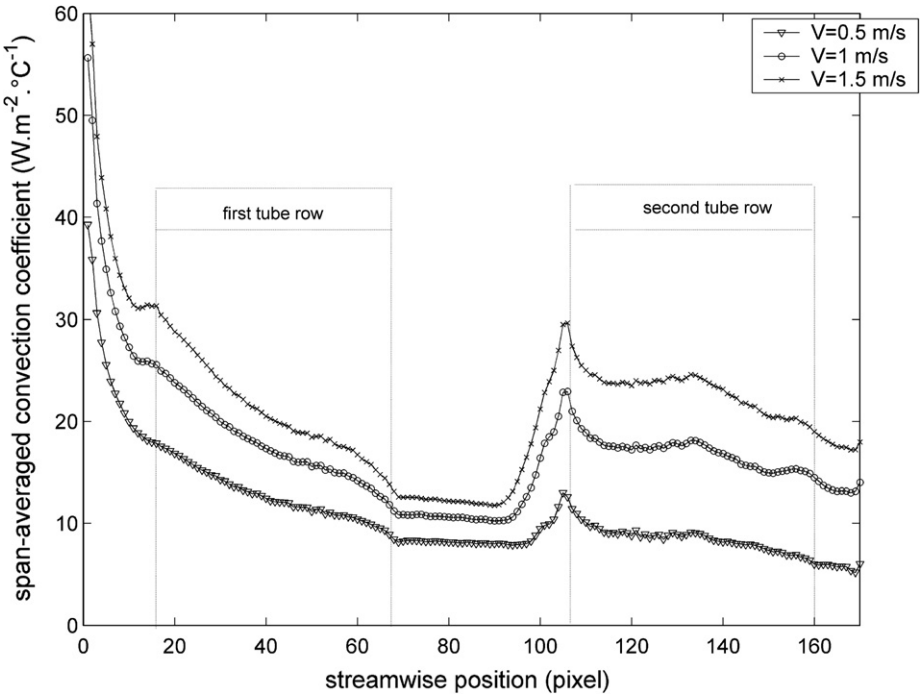

Fig. 15. Span-averaged coefficient for three different frontal velocities with $E = 7$ mm.

increases with the frontal velocity increase. This is particularly obvious for the second tube-row. Such results illustrate the growing influence of HSV structure on heat transfer in plate/fin-tube assembly. Fig. 16, that presents the profile of heat transfer coefficient along line A (see Fig. 8), strikingly shows the influence of the HSV in front of second tube row.

5.3. Variation of fin spacing

Investigations of the influence of fin spacing on heat transfer have also been performed. When the fin spacing increases, keeping constant the frontal airflow velocity, the behaviour of the heat transfer coefficient is not as simple as it seems. Two contrary phenomena occur. In a first

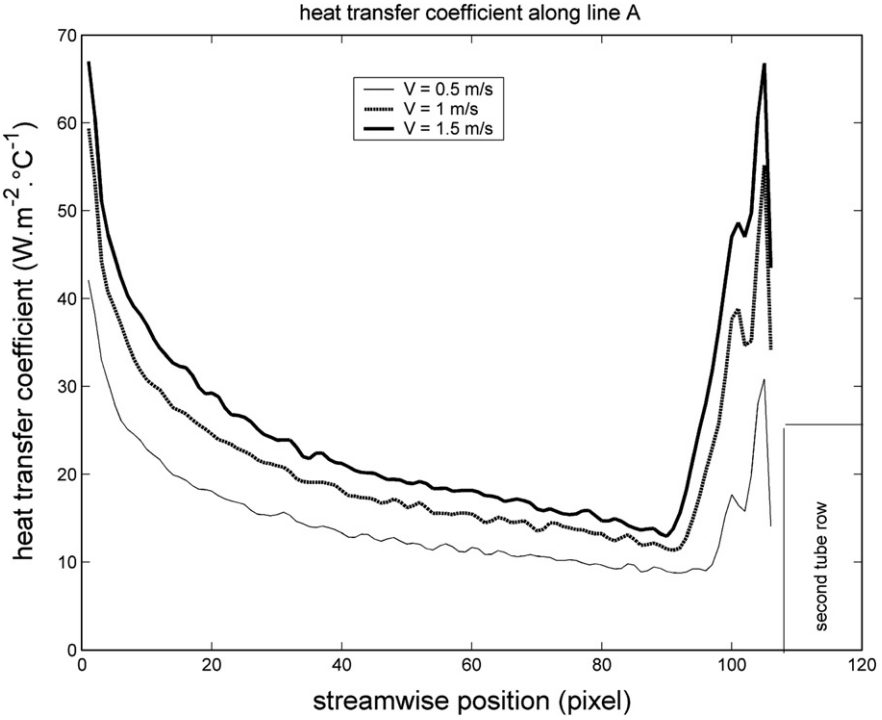

Fig. 16. Heat transfer coefficient distribution along line A (see Fig. 8) for three different velocities.

way, within the channel duct flow (central area with no major influence of the tubes), when the channel height decreases the convection coefficient increases. This is again a result of the Reynolds analogy. In a second way, when the channel height increases the HSV strength of the two-tube rows increases, bringing on locally high heat transfer. This last phenomenon remains again preponderant. In Fig. 17 we can see that, at the inlet of the channel, the lower channel height ($E/D = 0.18$) gives the higher heat transfer because of the first phenomenon. After the first tube row, the heat transfer increases for the higher channel height (due to the growth of HSV) and heat transfer becomes more important for $E/D = 0.31$. We can also see just behind each row of tubes that heat transfer is lower for the higher channel height. This can be explained viewing the heat transfer coefficient spatial distributions (not present here): the wake zone is slightly enlarged for this configuration decreasing heat transfer.

6. Experimental uncertainties

Uncertainties in the reduced data were estimated using standard methods (Moffat, 1988). Calculations were performed to show that natural convection had a negligible effect on results. Uncertainty analysis of each individual parameter measured was based on the instrument resolution. When the parameter is a thermo-physical property, the uncertainty calculation is based on the value given by the furniture supplier. The values of uncertainty for different parameters are given in Table 1. The root mean square (RMS) uncertainty of local heat transfer coefficient was calculated by using the uncertainties of the measured data given in Moffat (1988)

Table 1
Uncertainty analysis

x_i	dx_i
$T_{(x,y)}$ (K)	±0.15
T_{ref} (K)	±0.2
ρ_f (kg m^{-3})	±15
Cp_f (kJ kg^{-1} K)	±15
λ_f (W m^{-1} K)	±0.01
ε (–)	±0.02
TTray (K)	±1

The value of uncertainty in average heat transfer coefficient was 7.5%.

$$\partial h = \left[\sum \left(\frac{\partial h}{\partial x_i}\, dx_i\right)^2\right]^{1/2} \tag{11}$$

where x_i stands for the measured variable used to calculate h and dx_i is the tolerance of the corresponding variables.

7. Conclusions

IR thermography has been employed to quantitatively evaluate the local heat transfer coefficient in a plate fin-tube assembly. The present method compared to standard LCM was shown to improve HTC determination, mainly because it takes into account lateral heat conduction fluxes within the fin. The potential of this method is illustrated by applying it to study local heat distribution on heat exchanger fins. The experimental study was performed on a specific test bench with a test model consisting in a plate and

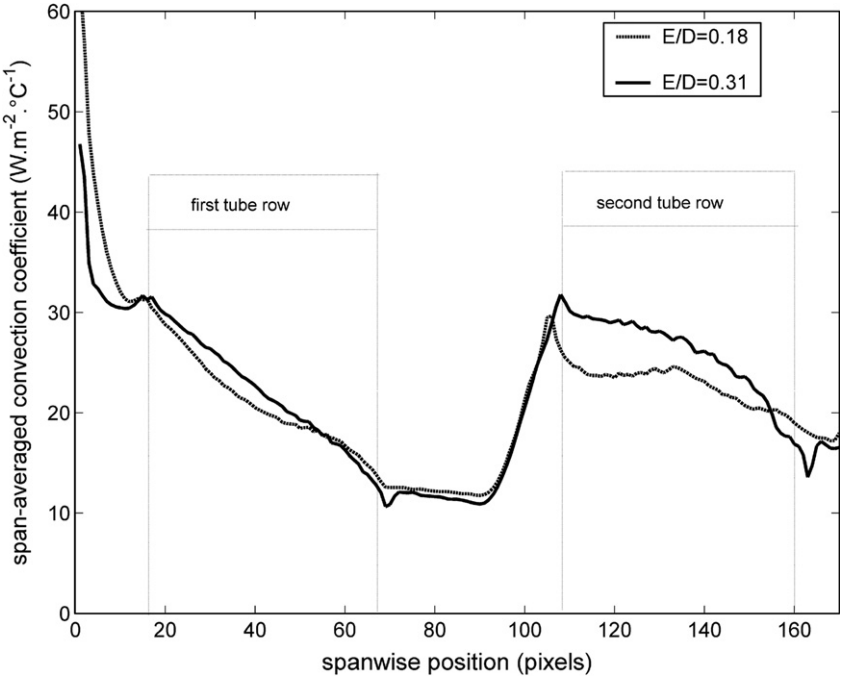

Fig. 17. Span-averaged coefficient for two channel heights.

two-tube row assembly. The following remarks can be stated:

- HSV structure is developed around the two-tube rows.
- Higher values of heat transfer coefficient have been found in front and around the second tube rows.
- The HSV structure around the second tube row is formed of two vortices.
- The two vortices structure cannot be seen using standard lumped capacitance method.

The results show clearly the capability and reliability of the method to measure convective heat fluxes due to complex flow topology. This technique is particularly interesting in investigating heat transfer distribution in complex geometries such as vortex enhanced heat exchangers.

Acknowledgement

Financial support for this research work has been granted by the European community (FEDER).

References

Astarita, T., Cardone, G., Carlomagno, G.M., Meola, C.A., 2000. Survey on infrared thermography for convective heat transfer measurements. Optics and Laser Technology 32, 593–610.

Ay, H., Jang, J.Y., Yeh, J., 2002. Local heat transfer measurements of plate finned-tube heat exchangers by infrared thermography. International Journal of Heat and Mass Transfer 45, 4069–4078.

Bejan, A., Sciubba, E., 1992. The optimal spacing of parallel plates cooled by forced convection. International Journal of Heat and Mass Transfer 35 (12), 3259–3264.

Bougeard, D., Vermeulen, J.-P., Baudoin, B., 1994. Spatial resolution enhancement of an IR system by image restoration techniques. In: Proceedings EUROTHERM Seminar 42, Quantitative Infrared Thermography QIRT 94 (Editions Européennes Thermique et Industrie), Sorrento, Italy, 23–26 August, pp. 3–8.

Incropera, F.P., Dewitt, D.P., 2002. The lumped capacitance method/transient conduction. In: Fundamentals of Heat and Mass Transfer. Wiley, New York, pp. 239–249.

Jacobi, A.M., Shah, R.K., 1995. Heat transfer surface enhancement trough the use of longitudinal vortices: a review of recent progress. Experimental Thermal and Fluid Science 11 (3), 295–309.

Khallaki, K., Russeil, S., Baudoin, B., 2005. Numerical study of the horseshoe vortex structure upstream a single plate-finned tube. International Journal of Heat and Technology 23 (1), 31–36.

Kim, J., Song, T., 2002. Microscopic phenomena and macroscopic evaluation of heat transfer from plate fins/circular tube assembly using naphthalene sublimation technique. International Journal of Heat and Mass Transfer 45, 3397–3404.

Kim, J., Song, T., 2003. Effect of tube alignment on the heat/mass transfer from a plate fin and two-tube assembly: naphthalene sublimation results. International Journal of Heat and Mass Transfer 46, 3051–3059.

Kim, Y.Y., Kim, K.S., Jeong, G.H., Jeong, S., 2006. An experimental study on the quantitative interpretation of local convective heat transfer for a plate fin and tube heat exchanger using the lumped capacitance method. International Journal of Heat and Mass Transfer 49, 230–239.

Moffat, R.J., 1988. Describing the uncertainties in experimental results. Experimental Thermal and Fluid Science 1, 3–17.

Morel, T., 1977. Design of two-dimensional wind tunnel contractions. Journal of Fluids Engineering, 371–378.

Nacer-Bey, M., Russeil, S., Baudoin, B., 2002. Experimental study of the effect of flow velocity and fin-spacing on the horseshoe vortex structure upstream of a one unit single-row plate-finned tube. In: Proceeding of Eurotherm 71 on Visualization, Imaging and Data Analysis in Convective Heat and Mass Transfer.

Taine, J., Petit, J., 2003. Transfert Thermiques Introduction aux Sciences des Transferts, 3ème ed. DUNOD, Paris, pp. 384–385.

Tiggelbeck, S., Mitra, N., Fiebig, M., 1992. Flow structure and heat transfer in a channel with multiple longitudinal vortex generators. Experimental Thermal and Fluid Science 5, 425–436.

Tourreuil, J., 2002. Etude des performances thermiques d'un échangeur de chaleur compact muni de promoteur de tourbillons – développement de techniques de mesures locales. Thèse de doctorat de l'Université de valenciennes et du Hainaut Cambrésis, France.